A Multi-Physics Framework for the Geometric Optimization of a Diaphragm Electrostatic Micropump

Emanuele Bertarelli[*,1], Raffaele Ardito[1], Elena Bianchi[1,2], Katia Laganà[1], Alberto Corigliano[1], Gabriele Dubini[1], Roberto Contro[1]
[1]Department of Structural Engineering, Politecnico di Milano
Piazza Leonardo da Vinci, 32 - 20133 Milano, Italy
[2]Department of Bioengineering, Politecnico di Milano
Piazza Leonardo da Vinci, 32 - 20133 Milano, Italy
*Corresponding author: bertarelli@stru.polimi.it

Abstract: In this work, an electrostatic diaphragm micropump is investigated by means of COMSOL Multiphysics 3.5. Due to the complexity of the device, results are obtained stepwise, performing preliminary analyses with simplified models and then by gradually introducing the different physics involved.
A fluid-dynamic model is adopted to evaluate the fluid flow characteristics inside the pumping chamber, in static conditions. In parallel, electro-mechanical quasi-static simulations are performed to evaluate the occurrence of membrane movement and pull-in phenomena. Finally, a simplified fully-coupled electrostatic-fluid-structure dynamic model is proposed, with the aim of appreciate the device performance in a true multi-physic and time-dependent framework.
The final goal of this research activity is the design of an innovative device, which enables proper fluid actuation at low voltage. The task at this stage is the definition of a numerical design approach to optimize the device geometry and actuation, enabling a proper fluid transport. This is intended to support future design process and prototype realization.

Keywords: Micropump, MEMS, Electrostatic actuation, Pull-in, Multiphysics.

1. Introduction

Recently, micropumping is emerging as a critical research area for many applications [1]. This is motivated in part by the need to develop pumping mechanisms for biological fluid handling, such as for polymerase chain reaction in DNA analysis (PCR), lab-on-a-chip, micro total analysis systems (μTAS), and drug delivery [2,3]. Microfluidic devices can be used to sample, trap, separate, sort, treat, detect and analyze biological materials and administer drugs, allowing for the controlled microscale fluid transport at flow rates ranging from nl/hrs to μl/min [4]. Moreover, micropumps are being considered for applications in the thermal management of electronic components. Liquid cooling in microchannels has the ability to increase power dissipation, and to reduce contact and spreading resistances by integrating the channels directly on the back side of the common flip-chip architecture [2].

Moreover, the perspective of taking advantage of micro-electro-mechanical systems (MEMS) technology to obtain affordable and reliable devices is of great interest. The direct integration with electronic components is a key feature for power supplying and control of the device, as well as for the straightforward embedding in the aforementioned electronic devices to be cooled or devices for fluid manipulation. This could be obtained by exploiting well-established silicon-based micro-fabrication processes, which are customarily adopted in integrated circuits technology [4,5].

In particular, the proposed devices is suitable to be produced by the surface micromachining process ThELMA, (Thick Epipoly Layer for Microactuators and Accelerometers) which has been developed by STMicroelectronics in order to manufacture in-silicon inertial sensors and actuators [6].

2. Device characteristics

A mechanical displacement micropump is here proposed and investigated. By definition, mechanical displacement micropumps use the motion of a solid (such as a gear or a diaphragm) or a fluid to generate the pressure difference needed to move a fluid. In particular, a dia-phragm micropump is considered, which is comprised of a pumping chamber connected to inlet and outlet valves necessary for flow control.

The electrostatic actuation is considered, since this choice shows some relevant advantages, such as low power consumption, fast response time and full MEMS compatibility [7]. It is worth noting that electrostatic actuation has received comparatively little attention in the recent micropump literature [1].

The first successful micropump with electrostatic actuation was built by Zengerle et al. [8]. The actuator was made of two silicon chips that embody the flexible pump diaphragm and a rigid counter electrode in a capacitor-like configuration. The application of an increasing voltage to the capacitor electrodes causes the electrostatic attraction of the pump diaphragm, which deflects towards the counter electrode. After discharge of the capacitor the pump diaphragm returns to its rest position. The major disadvantage of that solution resulted from the small stroke volume, partially balanced by high operation frequencies. Moreover, high voltages were requested for actuation, with a consequent charge build-up and efficiency loss in long-term operation.

The geometry here proposed for the micropumping device is reported in Figure 1 [6]. A circular pumping chamber with radius R = 2 mm and h = 10 μm height is designed. Inlet and outlet channels have the same depth of the chamber, a width b = 800 μm and a length L = 1 mm. Membrane thickness h_m ranging from 20 to 50 μm and capacitor electrode spacing h_c ranging from 4 and 10 μm are then evaluated in a parametric study. The space between electrodes is assumed to be filled of a dielectric, namely air. The actuation voltage is fixed at V = 60 V.

Inlet and outlet ports are placed along the perimeter of the pumping chamber, in diametrically opposite positions.

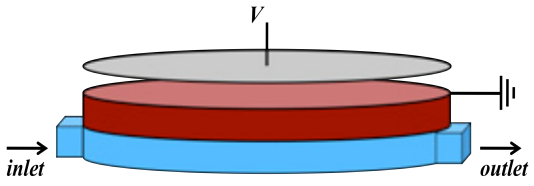

Figure 1. The proposed micropumping device geometry (not to scale). Condenser (upper gray plate), membrane (in red) and pumping chamber (in blue) are represented. Inlet and outlet valves are not reported.

In the filling phase, voltage is applied to the counter electrode and the diaphragm deflects under the electrostatic force acting on it. The pumping chamber expands, resulting in a corresponding decrease in chamber pressure (expansion stroke). When the inlet pressure is higher than the chamber pressure, the inlet valve opens and liquid fills the expanding chamber.

When the voltage is removed, the membrane bounces back. This increases the pressure in the pumping chamber (compression stroke), whereby liquid is discharged through the outlet valve. In fact, the driving force in the emptying phase is given by the elastic recovery of the membrane.

3. Modelling

To the purpose of this investigation, both 3D and 2D models are adopted. Hexahedral and quadrilateral elements with second order shape functions are used for structural, electrostatic and fluid domains.

The membrane is made of polysilicon, modelled as isotropic linear elastic (Young's modulus E = 160 GPa, Poisson's ratio υ = 0.22, density ρ = 2320 Kg/m^3). Large deformation formulation is used. For the sake of simplicity, the counter-electrode and the remaining chamber walls are assumed to be rigid and they are not modelled. The space between electrodes is assumed to be filled by air (permittivity ε = $8.8542 \cdot 10^{-12}$ F/m). The pumped fluid is assumed to be water (density ρ_w = 1000 Kg/m^3, viscosity μ_w = 0.001 Pa·s), and modelled as incompressible, homogeneous and Newtonian.

The mesh movement is described by the arbitrary Lagrangian-Eulerian method. Time-dependent solution is obtained by an implicit solver (backward Euler integration).

The continuum hypothesis for fluid modelling is still valid at the size scales of these devices. However, it should be underlined that peculiar physical effects become important as surface forces dominate over body and inertial forces. Then, the main consequence of miniaturization for micropumping devices is that surface tension becomes proportionally more significant than inertial forces. This might be relevant in the evaluation of micropump performances [4].

Where required, suitable boundary conditions are defined between adjacent domains, in terms of electrostatic force and displacements for the electro-mechanical interaction, as well as boundary velocity and fluid load for the fluid-structure interaction. Ideal valves are considered, i.e. with no pressure drop across the fully open structure and no leakage if valve is closed.

4. Results

4.1 Fluid-dynamic simulations

As a first step of the investigation, a fluid-dynamic 3D model allowed for the evaluation of the pressure drops across the device in static conditions. Although these results cannot be directly correlated to the fluid flow behaviour in dynamic conditions, this approach gives some useful indications with respect to the geometry according to pressure drop estimate.

The imposed flow rate at the inlet boundary is 10 μl/min, in line with the values suggested for micropumps for biomedical applications [9,10]. Accounting for the symmetry of the pumping chamber, only one quarter of the model is represented.

In Figure 2, the pressure map is represented, evaluated at the midplane of the fluid domain. As expected, from the fluid-dynamic standpoint the most critical areas are located next to the sharp corners between the chamber and the channels. Thus, the influence of the chamfer angle (Figure 3) on the pressure drop has been investigated (Table 1), for values ranging from 0° (straight channel) to 60° (tangent to the pumping chamber wall).

By splitting the fluid domain, it is possible to separate the pressure drop contribution due to the microchannels and to the pumping chamber. The pressure drop per unit length obtained for the microchannel from numerical simulations is $\Delta p_L \cong$ 2545 Pa/mm.

This value can be compared with the analytical one, computed by applying the relation

$$Q = \frac{h\, b^3}{12\, \mu_w} F\,(b/h)\, \Delta \tilde{p}_L \qquad (1)$$

where *h* and *b* are the height and the width of the microchannel, respectively. This relation is derived from the Navier-Stokes equations. It holds for channels whit *b/h* > *4.5* [11,12].

The function *F* can be expressed as

$$F\,(b/h) = 1 - \frac{192\, b}{\pi^5\, h} \sum_{i=1,3,5,..}^{\infty} \frac{\tanh(i(\pi h/2b))}{i^5} \qquad (2)$$

By applying eq. (1), the pressure drop is $\Delta \tilde{p}_L \cong$ 2540 Pa/mm.

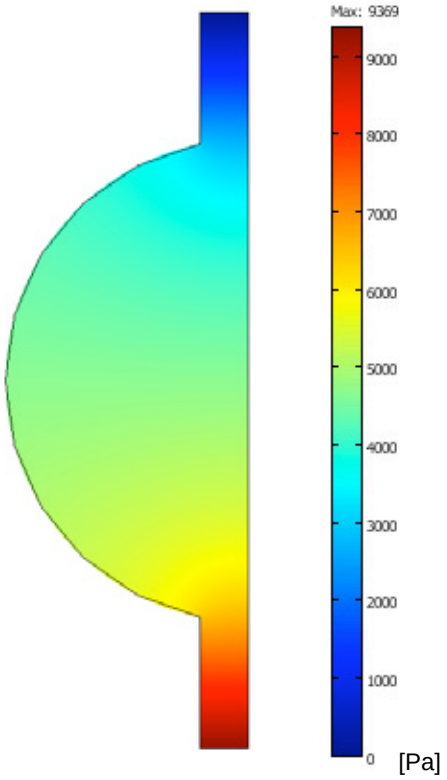

Figure 2. Pressure map at the midplane.

.

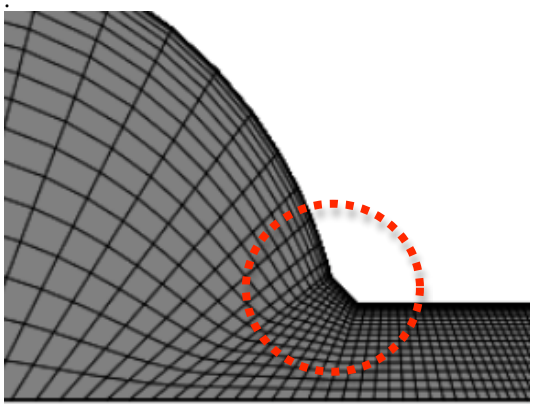

Figure 3. The chamfer angle, detail of the mesh.

Chamfer angle	*ΔP (Pa)*	*Δ%*
0° *(straight)*	9369	---
15°	9320	-0,5
30°	9275	-1,0
45°	9227	-1,5
61° *(tangent)*	9154	-2,3

Table 1. The influence of the chamfer angle on the pressure drop, for the full device, expressed in Pa and as variation with respect to the straight configuration.

4.2 Electro-mechanical simulations

An axisymmetric electro-mechanical finite element model is defined, with the aim to obtain the membrane deformed configuration in quasi-static conditions. A parametric study with respect to capacitor height (h_c) and membrane thickness (h_m) is performed, for a fixed applied voltage of $V = 60$ V.

The problem is first considered as loosely-coupled. The electrostatic domain is solved, and subsequently the electrostatic load is applied to the solid domain. The membrane deflection obtained with this method is in fact equivalent to the approximated analytical solution, which has been presented in [6].

The equivalent pressure given by the electrostatic force, assuming infinite parallel rigid plates, is

$$p_{es}^{th} = \frac{\varepsilon V^2}{2\,h_c^2} \tag{3}$$

Eq. (3) is a lower limit for the electrostatic pressure acting on the membrane, since the effective gap is given by $h_c - f(r,t)$, where f is the membrane deflection.

By applying the Kirchhoff classical thin plate theory, it is straightforward to obtain the expression for the maximum deflection (at membrane midpoint) for a clamped circular plate subject to the pressure given by eq. (3):

$$f_{max}^{th} = \frac{3}{32} \cdot \varepsilon V^2 \cdot \frac{1-\upsilon^2}{E} \cdot \frac{R^4}{h_m^3\, h_c^2} \tag{4}$$

Subsequently, the effective electrostatic load is obtained by solving the fully-coupled electro-mechanical problem.

As expected, numerical simulations where the equivalent pressure p_{eq} is imposed, exactly correspond to the analytical solution. In fact, the error committed adopting eq. (4) is found to be greater than 10% even for small deflections, i.e. $f_{max} \cong h_c/10$. Results are graphed in Figure 4. Missing points are those for which pull-in occurred and a stable configuration cannot be determined (see Section 4.3).

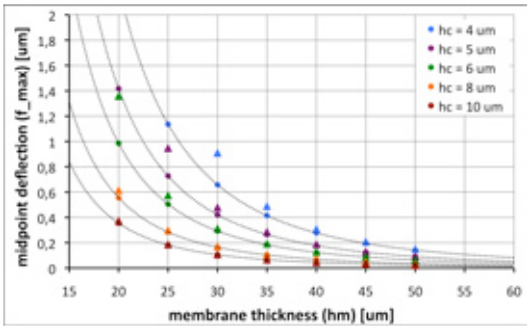

Figure 4. Membrane midpoint deflection as a function of membrane thickness, for different capacitor height. Dashed lines: analytical solution; bullets: numerical simulations with p_{eq}; triangles: fully-coupled electro-mechanical numerical simulations.

From the fully-coupled model, the stroke volume (i.e. the pumping chamber volume variation) is calculated (Figure 5). Stroke volume reaches a value of few nanoliters, in line with other devices studied for similar applications [9].

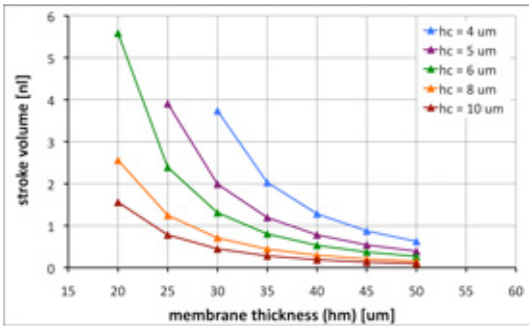

Figure 5. Micropump stroke volume as a function of membrane thickness, for different capacitor height. Data are obtained from fully-coupled electro-mechanical static simulations.

4.3 Pull-in simulations

Pull-in (or "jump-to-contact" instability) is a relevant feature in electrostatically actuated micro-electro-mechanical systems, which occurs when applied voltages are increased beyond a critical value.

In this situation, there is no longer a steady state configuration of the device and the membrane collapses onto the ground plate. This may be accounted as the limit of the stable operation regime for the micropump.

With the axisymmetric fully-coupled electro-mechanical model the pull-in voltage V_p is estimated for different h_c and h_m, performing a two-step procedure. The value is preliminary located increasing the applied voltage with 1 V steps, then a more accurate simulation with 0.001 V steps is carried out in proximity of the previously identified voltage. Results are reported in Figure 6. Pull-in occurs when the midpoint deflection reaches a limit value, which is for all configurations $f_{lim} \cong 0.46 \cdot h_c$. This value differs substantially from the theoretical one for infinite and perfectly plane plates which is $f_{lim} \cong 0.33 \cdot h_c$ [13].

4.4 Electrostatic-fluid-structure dynamic simulations

The further step is the realization of a fully-coupled dynamical model, which describes the fluid behaviour into the chamber, during the pumping. The fluid domain is then added to the numerical simulation. Open boundary conditions are imposed for inlet and outlet.

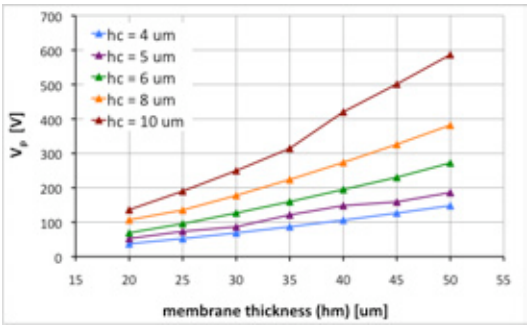

Figure 6. Pull-in voltage as a function of membrane thickness, for different capacitor height.

Three sequential simulations are performed, representing three steps of functioning of device, each one 1 second long. During the first step, a linearly increasing voltage is applied to the electrode reaching the maximum value of 60 V. On the second step, the voltage is held constant at the maximum value, allowing the device reaching equilibrium conditions. Finally, the capacitor is deactivated, to obtain the emptying of the pumping chamber as a consequence of membrane elastic recovery.

In order to account for inlet and outlet in the pumping chamber in the simplest way, a bi-dimensional plane strain model is defined, and a diameter slice of the device is represented. Since the plane strain formulation presents a membrane flexural stiffness lower than the clamped circular plate, a scaling is necessary to obtain the same deflections as the axisymmetric formulation. A straightforward solution is to scale Young modulus, defining an equivalent modulus such that the maximum deflection obtained in plane strain simulations is the same that in the previously performed axisymmetric analysis. This way, an equivalent membrane deflection is obtained.

With the additional condition on the thickness $t = \pi R/2$, the initial volume V_0 of the chamber is preserved. The volume $V(t)$ during actuation is in general larger, due to the different membrane deformed configuration.

A solution to overcome this volume mismatch might be a proportional scaling with respect to the final volume V_f obtained in electro-mechanical static simulations. Anyway, at this stage, the previous strong assumptions make this model suitable only for a qualitative evaluation of the device in a dynamic framework

In Figure 7, electrode voltage, chamber volume, inflow and outflow are reported for a pumping cycle, for a device with $h_m = 30$ µm and $h_c = 6$ µm. The linearly increasing voltage generates a smooth filling. A complete filling is obtained after a hold of approximately 100 ms.

The emptying phase is extremely fast. The abrupt membrane release generates a fast stroke, with a very high outflow peak. This was expected, as a consequence of the stepwise voltage reduction and the open boundary condition imposed at the outlet. This means that no resistance is opposed to the outflow of fluid, which is expelled from the chamber in a short time: Figure 8 shows that the emptying transient phase lasts for less than 50 ms.

5. Conclusions

A preliminary investigation by means of numerical methods has been performed on an electrostatic micropumping device. It gives suggestions on the development of the device, in terms of working principle, geometric parameters, actuation voltage, and provides also useful indications on further analyses to be performed and on prototype realization.

The finite element models which have been defined show a very good agreement with the reference closed form solutions, where those are available. For the fully coupled problem, however, the numerical solution is mandatory, and showed a significant difference with the results of the loosely coupled analytical formulation.

While for the reported configuration values of h_m = 20 ÷ 30 μm and h_c = 4 ÷ 6 μm have been proven to be the most suitable, a wider range of actuation voltage should be investigated. A strong attention should be paid to pull-in phenomena, with the aim to control this feature and eventually to take advantage of it (since in that case a larger stroke volume is obtained). To this purpose, an analysis should be performed to evaluate the adhesion (stiction) of the membrane and the membrane release after capacitor deactivation.

The chamfer angle in the pumping chamber inlet and outlet shows a negligible effect on the pressure drop across the device in static conditions.

The next step will be the creation of a complete 3D model, by implementing suitable boundary conditions for inlet and outlet valves and peculiar microscale effects. The final goal is to develop a computational tool, which allows the analysts to forecast the device behaviour in a parametric framework.

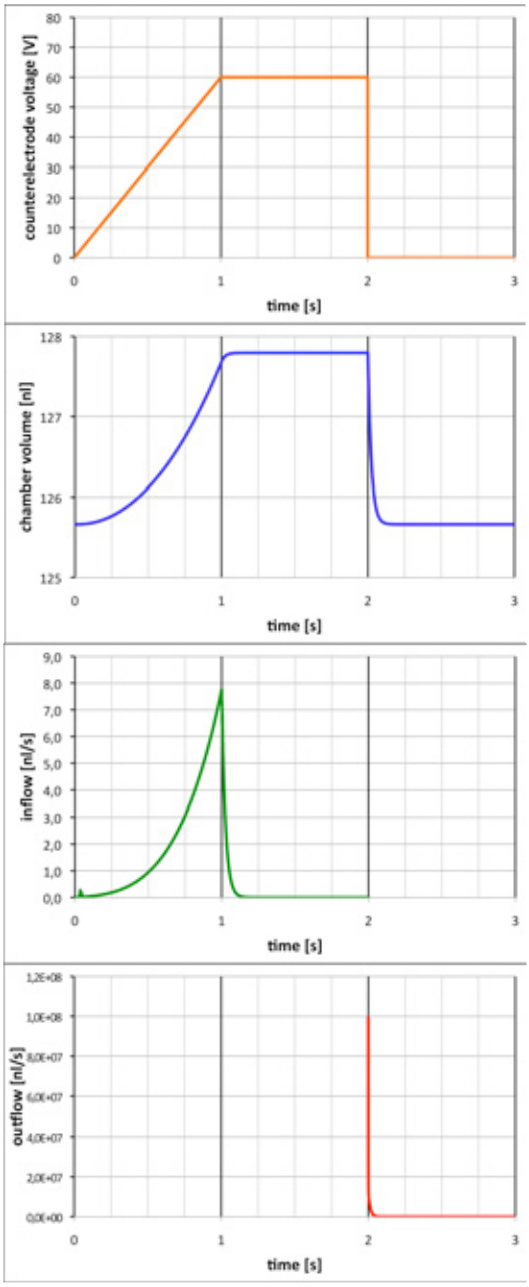

Figure 7. Results from the fully-coupled dynamical model in plane strain approximation, for h_m = 30 μm and h_c = 6 μm. One pumping cycle is reported.

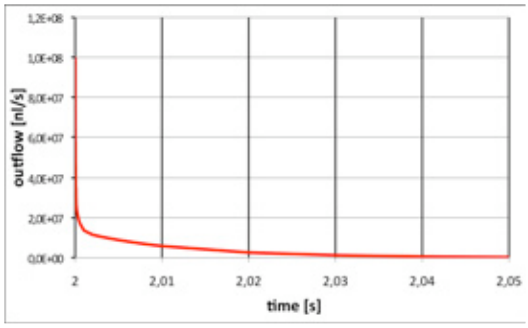

Figure 8. Outflow on the initial phase of membrane release, time scale magnification from Figure 7.

6. References

1. B.D. Iverson, S.V. Garimella, Recent advances in microscale pumping technologies: a review and evaluation, *Microfluid Nanofluid*, **5**, 145–174 (2008)
2. C. Zhang, D. Xing, Y. Li, Micropumps, microvalves, and micromixers within PCR microfluidic chips: Advances and trends, *Biotechnology Advances*, **25**, 483-514 (2007)
3. A. Nisar, N. Afzulpurkar, B. Mahaisavariya, A. Tuantranont, MEMS-based micro-pumps in drug delivery and biomedical applications, *Sensors and Actuators B*, **130**, 917–942 (2008)
4. W. Wang, S.A. Soper, *Bio-MEMS Technologies and Applications*, CRC Press, (2007)
5. J.G. Korvink, O. Paul, *MEMS: A Practical Guide to Design, Analysis, and Applications*, William Andrew Publishing - Springer (2006)
6. E. Bertarelli, R. Ardito, M. Cioffi, K. Laganà, F. Procopio, L. Baldo, A. Corigliano, R. Contro, G. Dubini, Design optimization of an electrostatic micropump: a multi-physics computational approach, *Proceedings of SEECCM 2009*, 181 & CD-ROM, Rhodes, Greece, 22-24 June (2009)
7. P. Woias, Micropumps - past, progress and future prospects, *Sensors and Actuators B*, **105**, 28–38 (2005)
8. R. Zengerle, H. Sandmaier, A Micro membrane pump with electrostatic actuation, *Proceedings of the MEMS '92*, 19-24, Travemünde, Germany, 4-7 February (1992)
9. M.M. Teymoori, E. Abbaspour-Sani, Design and simulation of a novel electrostatic peristaltic micromachined pump for drug delivery, *Sensors and Actuators A*, **117**, 222-229 (2005)
10. R.S. Shawgo, A.C. Richards Grayson, Y. Li, M.J. Cima, BioMEMS for drug delivery, *Current Opinion in Solid State and Materials Science*, **6**, 329-334 (2002)
11. D. De Bruyker, R. Puers, Experimental characterization of the reference channel of a differential pressure sensor using pressure shock waves, *Journal of Micromechanics and Microengineering*, **11**, 390-396 (2001)
12. F.M. White, *Viscous Fluid Flow*, section 3-3.3, McGraw-Hill, New York (1991)
13. V. Rochus, D.J. Rixen, J.-C. Golinval, Electrostatic coupling of MEMS structures: transient simulations and dynamic pull-in, *Nonlinear Analysis*, **63**, e1619-31633 (2005)